

Automatic Mapping of Valley Networks on Mars

I. Molloy^a and T. F. Stepinski^{b,*}

^a*Department of Computer Science, Purdue University, 250 N. University St.,
West Lafayette, IN 47907, USA*

^b*Lunar and Planetary Institute, 3600 Bay Area Blvd., Houston, TX 77058, USA*

Abstract

Martian valley networks bear some resemblance to terrestrial drainage systems, but their precise origin remains an active research topic. A limited number of valley networks have been manually mapped from images, but the vast majority remains unmapped because standard drainage mapping algorithms are inapplicable to valleys that are poorly organized and lack spatial integration. In this paper we present a novel drainage delineation algorithm specially designed for mapping the valley networks from digital elevation data. It first identifies landforms characterized by convex tangential curvature, and then uses a series of image processing operations to separate valleys from other features having a convex form. The final map is produced by reconnecting all valley segments along drainage directions. Eight test sites on Mars are selected and manually mapped for valley networks. The algorithm is applied to the test sites and delineated networks are compared to mapped networks using a series of quantitative quality factors. We have found a good agreement between delineated and mapped networks. In the process of comparing manual and delineated networks some shortcomings of manual mapping became apparent. We argue that delineated networks are indeed of better quality than the networks manually mapped from images. Although the algorithm has been developed to study Martian surface, it may also be relevant to terrestrial geomorphology.

Key words: Drainage delineation, Image processing, Digital topography models, Automated techniques, Mars

* Corresponding author. Tel.: +1 281 486 2170; fax: +1 281 486 2162.
Email address: tom@lpi.usra.edu (T. F. Stepinski).

1 Introduction

Valley networks are common geomorphic features on Mars that are visually reminiscent of terrestrial river systems. This resemblance gave rise to a suggestion (Masursky, 1973; Milton, 1973) that they were incised by surface runoff and are remnants of once active drainage networks. Runoff erosion requires a widespread and sustained precipitation, conditions that are impossible to maintain by the present-day Martian atmosphere. However, the majority of valley networks are located in Martian southern highlands, a region that experienced little geologic change for the past 3.5 billion years. Thus, valley networks may indicate that warmer climate occurred early in Mars history. Determining the origin of valley networks would have significant consequences for our understanding of the history of water and climate on Mars with implications for exobiology models.

To enable the study of valley networks, they first need to be mapped. Mapping of valley networks is traditionally done manually via interpretation of images. Baker and Partridge (1986) mapped and collected image-derived attributes for 24 small valley networks. Cabrol and Grin (2001) mapped another 71 small valley networks. Carr (1995) mapped over 800 networks of all sizes; it's the most widely used database of Martian valley networks. Finally, van Gasselt et al. (2002) mapped and classified 1100 valley networks using imagery and topographic data. Because the manual methodology is labor intensive and slow, only a small fraction of networks have been mapped. Moreover, manual mapping is subjective, the results vary depending on image quality and interpretation criteria. For example, Hynek and Phillips (2001) has mapped five regions previously mapped by Carr (1995). In both cases images with resolution of 256 pixels/degree were used yet networks mapped by Hynek and Phillips are about an order of magnitude denser than networks mapped by Carr. The authors attribute this difference to better quality and consistency of their imagery data, but subjectivity in image interpretation must also play a role. Automating the process of mapping the valley networks would significantly speed up the rate of building datasets and provide means for objective and repeatable analysis.

In terrestrial context, drainage networks are automatically mapped by a computer algorithm that uses topography data in the form of digital elevation models (DEMs). A DEM is a raster dataset where each pixel is assigned an elevation value. The most popular algorithm is based on the concept of local drainage directions; each pixel in a DEM is assigned a drainage pointer to one of neighboring pixels in the direction of the steepest slope (O'Callaghan and Mark, 1984). Using these pointers all pixels in a DEM could be organized into a number of binary tree data structures with the leaves of the tree located at the ridges and the roots of the trees located at watershed outlets. The pixels

underlying a tree form a drainage basin drained by a network constructed by pruning the tree according to a channelization criterion. The pruning is necessary because not all runoff results in surface incision. Number of channelization criteria, based on either physical or phenomenological reasoning, have been applied to map drainage networks (O’Callaghan and Mark, 1984; Tarboton et al., 1991, 1992; Montgomery and Dietrich, 1992). Variants of such an algorithms has been implemented in software packages such as ESRI’s ArcGIS, Rivix’s RiverTolls, or TauDEM.

Assuming that Martian valley networks represent ancient drainage systems, the drainage direction algorithm could be applied, in principle, to map the valleys. However, a straightforward application of such an algorithm to Mars is not feasible. First, unlike the terrestrial landscape, the Martian terrain is not naturally drainable because of the existence of the craters and other pits that break Martian topography into a large number of small internal drainage basins. Many craters are features superimposed over valleys destroying the original drainage integration. Second, the valley networks lack spatial integration, dissected areas are commonly separated from each other by undissected areas of similar or bigger size (Carr, 1996). Stepinski and Collier (2004) had addressed the craters issue by selectively flooding the terrain. The “flooding” is a terrain modification procedure wherein pits in the DEM are raised to the level of the top off point. In terrestrial context the purpose of flooding is to remove artifacts that interfere with the routing of flow across a DEM and to make it completely drainable. In Martian context, Stepinski and Collier had designed a procedure of flooding craters that prevent flow continuity but excluding large, contaminant craters from being incorporated into drainage basins. This facilitates mapping drainage network of a single, selected drainage basin, but the method cannot be used to map valley networks in an arbitrary site. The lack of integration issue cannot be addressed within a framework of drainage directions algorithm, because the algorithm produces spatially uniform networks regardless of spatial distribution of an actual drainage system.

In this paper we present a procedure for automated mapping of valley networks in an arbitrary site as represented by its DEM. The procedure relies on a combination of methods from fields of digital terrain analysis and image processing. The core idea is to identify valleys pixel-by-pixel using terrain morphology instead of terrain connectivity as in the drainage directions algorithm. The terrain analysis part of our procedure identifies segments of the terrain with convex (concave upward) morphology. Such segments, identified by positive tangential curvature are the areas where flow accumulates, and thus, many of them are the constituent parts of valley networks. The image processing part of our procedure is designed to separate segments constituting valleys from segments constituting other Martian landforms that are also characterized by convex tangential curvature.

Table 1
Names, locations, and attributes of test sites

site #	Name	lat(L)	lat(U)	lon(L)	lon(R)	Width	Height	Area	Images
1	Locras Valles	6.0	11.0	45.0	49.0	474	593	70.3	18
2	Pollack	-11.1	-6.7	27.8	34.8	593	593	87.9	15
3	Evros Vallis West	-15.8	-10.2	10.8	18.0	853	664	141.6	25
4	Evros Vallis North	-11.3	-5.3	11.6	18.6	829	711	147.4	31
5	Dawes East	-8.4	-3.2	42.5	47.9	640	616	98.6	18
6	Millochou West	-23.4	-16.9	84.7	91.7	829	770	159.6	29
7	Millochou South	-26.0	-20.0	85.0	91.0	711	711	126.4	28
8	Naktong Vallis	1.0	9.0	28.0	36.0	948	948	224.7	40

The aim of this paper is to provide a detailed description of proposed, curvature-based algorithm for mapping Martian valley networks and to investigate its utility. To this end we illustrate each step of an algorithm on a test site, and use eight test sites to compare the mapping of the valleys produced by our algorithm to manual mapping.

2 Description of test sites and data

The eight areas selected as test sites for our valley mapping algorithm are all located on the portion of Martian surface that has been dated from an early period in Mars history and exhibits clearly visible valley networks. The sites are listed in Table 1. The name in the second column of Table 1 is the name of the nearest prominent landscape feature. The columns three to six list the site’s location: latitude of the lower edge, latitude of the upper edge, east longitude of the left edge, and east longitude of the right edge, respectively. The columns seven and eight list the site’s width and height in the pixels units. The ninth column gives the site’s area in the units of 10^3 km^2 . Finally, the last column gives the number of images used to construct the mosaic of the site (see below). The sites’ sizes are of the order of 100 km^2 , approximately the size of the state of Ohio. The DEMs for these sites are constructed from the Mars Orbiter Laser Altimeter (MOLA) Mission Experiment Gridded Data Record (MEGDR) (Smith et al., 2003) that has resolution of $1/128$ degree, or $\sim 500 \text{ m}$ at the equator.

In order to obtain the ground truth maps of valleys in those sites, we have constructed mosaics of 100 m/pixel images, taken during daytime by the THEMIS instrument aboard the Mars Odyssey spacecraft (Plaut et al., 2003), to cover

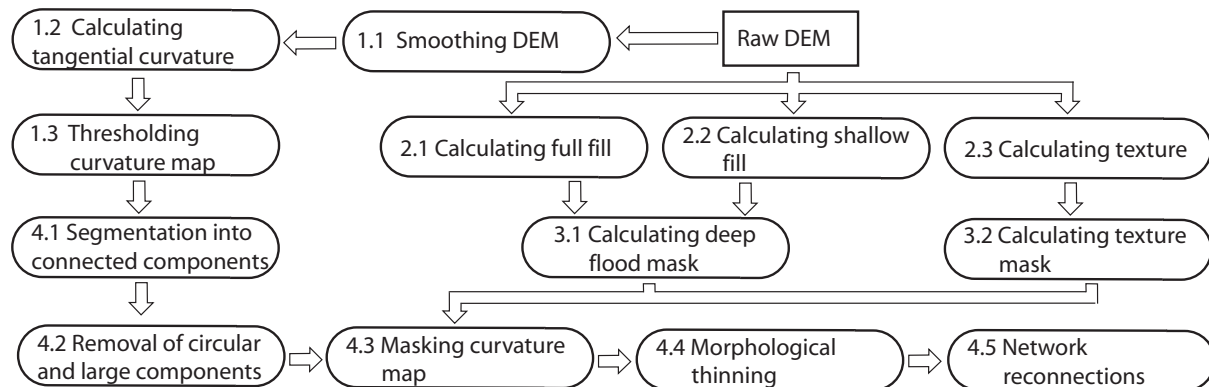


Fig. 1. A schematic view of the computational process leading to an automated classification of landforms.

the areas of the test sites listed in Table 1. The mosaics have been coregistered with the corresponding DEMs and used to manually map the valleys. These maps are used to assess the accuracy of our mapping algorithm.

3 Methodology

Fig. 1 shows a schematic diagram of overall organization of our valleys mapping algorithm. It consists of several major modules devoted to calculation of tangential curvature (tasks labeled 1 at Fig. 1), calculation of other terrain parameters (2), calculation of masks for an image of thresholded tangential curvature (3), and the final construction of mapped valley networks (4), respectively. Subsequent subsection describe these modules in detail using the test site # 2 (Pollack) to illustrate how they work. This site features a couple of large conjoined craters located at the terrain elevated above the surrounding plain. The valley networks are clearly visible on the sides of the elevated structure.

3.1 Tangential curvature

Using terrain morphology to extract drainage networks has been proposed before in terrestrial context. Peucker and Douglas (1975) has proposed an algorithm for an identification of convex pixels in a DEM. Although efficient, this algorithm yields broken and inconsistent drainage segments in contrast to the set of connected and organized drainage paths produced by the less efficient drainage direction algorithm. Band (1986) has improved on the Peucker and Douglas algorithm by employing morphological thinning and reconnection operations. His method worked well in rugged terrain, but worse in less rugged terrain or in the case of more complex pits. More recently, Tarboton

and Ames (2001) had developed an algorithm that combines the Peucker and Douglas method with the drainage direction method in order to achieve adaptability to spatial variability in drainage density. Howard (1994) used gradient divergence of landscape elevation field as a proxy for convexity of the local terrain and applied it to define drainage network.

We have found that, in Martian context, neither of these approaches constitutes a basis for a successful valleys mapping algorithm. Instead, we have found that tangential curvature κ_t is the best terrain parameter to delineate the valleys. The $\kappa_t(x, y)$ is a curvature measured in the direction of tangent to contour at a given point (Mitasova and Hofierka, 1993) and thus its value is directly related to terrain ability to diverge or converge water flow over the surface. The positive values of κ_t indicate convex forms and converging flow, whereas negative values of κ_t indicate concave forms and diverging flows. The valley networks have convex forms and could be identified by positive values of κ_t . Denoting the elevation field by $z = f(x, y)$, the κ_t is given by

$$\kappa_t = \frac{f_{xx}f_y^2 - 2f_{xy}f_xf_y + f_{yy}f_x^2}{(f_x^2 + f_y^2)\sqrt{1 + f_x^2 + f_y^2}} \quad (1)$$

Note that κ_t has the same spatial distribution of convex and concave areas as the better known planar curvature, but different values.

The Martian DEMs lack smoothness because of their limited accuracy, resolution, interpolation, and the true roughness of Martian terrain. Therefore, calculation of κ_h using finite differences approximation on a 3×3 moving window, as is customary in terrain analysis software packages, is not feasible because it produces noisy results. We first smooth $f(x, y)$ using a mean value of f calculated over a circular moving window of radius equal to 5 pixels. We use the smoothed elevation field to fit two-dimensional, second order polynomials to local patches of elevation data contained in a 5×5 moving window. The κ_t is calculated analytically using (1) with function $f(x, y)$ replaced by a local polynomial approximation. This procedure, similar to that employed by Roering et al. (1999), results in relatively smooth field of κ_t .

To obtain the first “draft” of valley networks map the curvature field is thresholded producing a binary image with pixels having $\kappa_t > \kappa_t^{\text{th}}$ labeled 1 and the remaining pixels labeled 0. Fig. 2 illustrates the results of curvature calculations for the test site. Panel (A) shows the visual rendering of the DEM and is shown for reference. The valleys are clearly identifiable in the DEM; their spatial distribution is variable with very few valleys located in the southern region of the site. Panel (B) shows the map of κ_t , the red-yellow-blue gradient indicates values of κ_t from the minimum of -0.09 to the maximum of 0.06. The values of κ_t are measured in units of (1/m). Majority of pixels are displayed

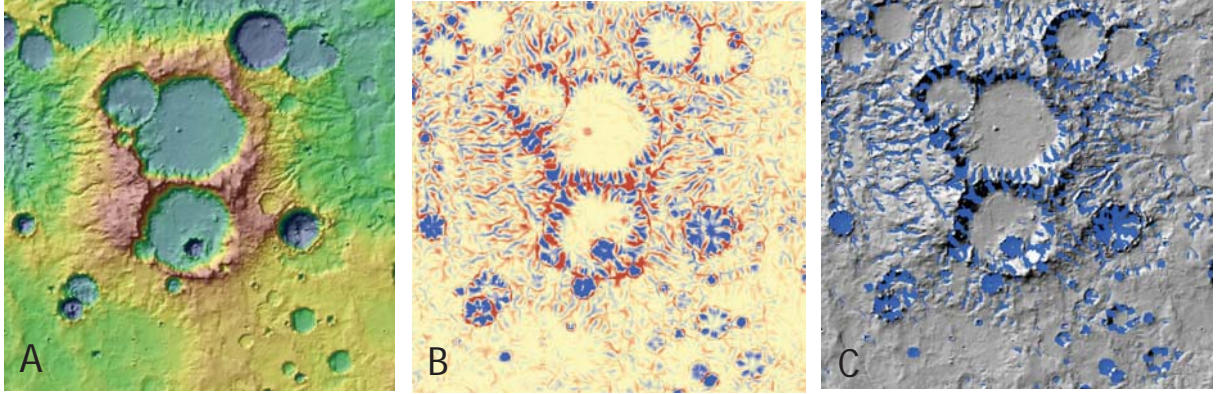


Fig. 2. (A) A shaded relief of the topography in the Pollack test site colored using elevation values, the blue-to-red gradient corresponds to low-to-high elevations. (B) The map of tangential curvature, blue corresponds to most convex forms, red corresponds to most concave forms. (C) Binary image of thresholded tangential curvature superimposed on shaded relief.

in yellow indicating near-zero values of κ_t ; these are regions characterized by flat contours. Pixels shown in red flag terrain with the most concave form of contours, whereas pixels shown in blue flag the terrain with the most convex forms of contours. Panel (C) shows in blue the part of the terrain for which $\kappa_t > \kappa_t^{\text{th}}$. We have set the value of κ_t^{th} to 0.003 in all our calculations. Comparing Figs. 2A and 2C it is clear that thresholded κ_t outlines valley networks, but it also outlines many other landforms. The remaining subsections discuss an array of techniques designed to separate the valleys from other landforms fulfilling the $\kappa_t > \kappa_t^{\text{th}}$ condition. Fig. 3 illustrates progressive separation steps.

3.2 Segmentation

The binary image of thresholded curvature (Fig. 2C) consists of many disconnected fragments. The thin elongated fragments are likely to indicate valleys, whereas more bulky fragments are likely to correspond to parts of craters and other landforms. We apply the connected components labeling algorithm (Chang et al., 2004) to the binary image of thresholded curvature in order to segment it into separate fragments. The perimeter, P , and area, A , of each fragment are calculated using an algorithm described by Michielsen and De Raedt (2001). These are used to calculate fragment's circularity $C = 4\pi A/P^2$, a measure of fragment's elongation. Circular fragments have values of C approaching 1, but elongated fragments have very small values of circularity. We eliminate all fragments characterized by $C > 0.3$ and $A > 20$ pixels, as they tend to delineate landforms other than valleys. Fig. 3A shows all fragments identified by the curvature criterion and Fig. 3B shows only the fragments fulfilling the circularity and area criteria. It is clear that segmentation has fil-

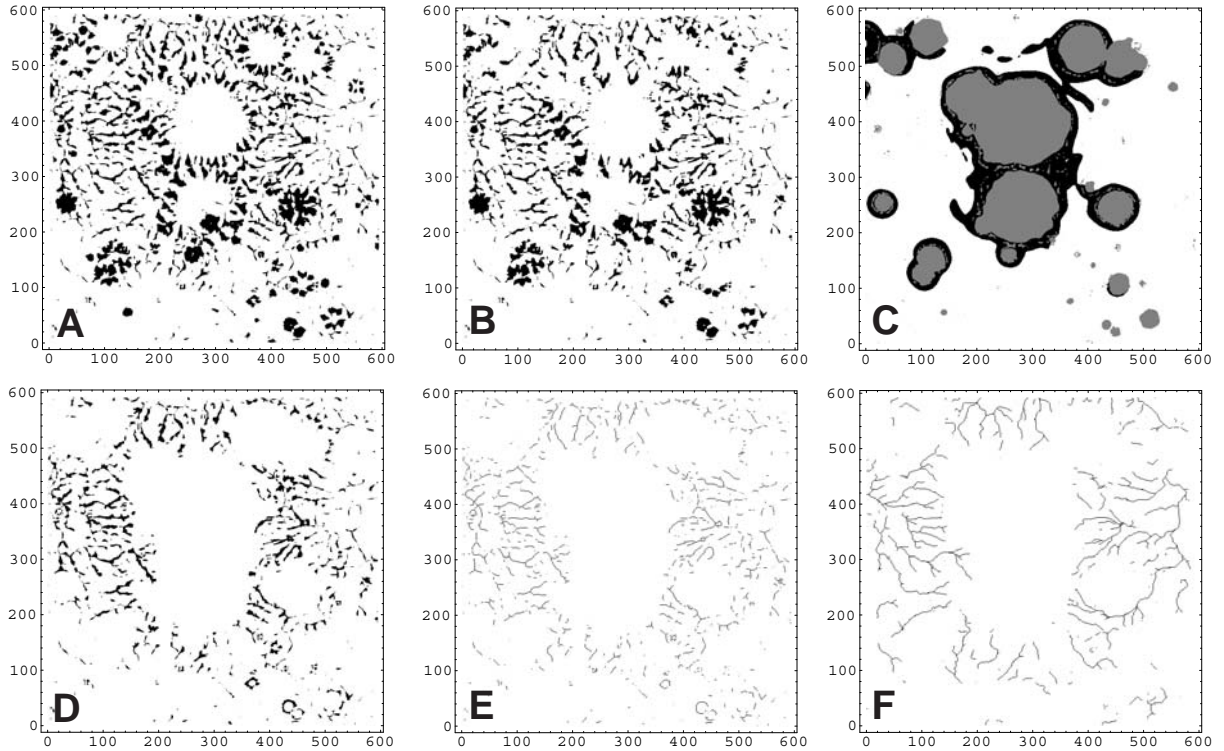


Fig. 3. (A) The binary image of thresholded tangential curvature, black pixels are places where the curvature criterion is fulfilled. (B) The binary image of curvature with circular and/or large fragments eliminated. (C) Craters’ mask, gray indicates the deep flood component, black indicates the texture component. (D) The binary image of curvature shown in panel B after applying the mask. (E) The binary image of curvature shown in panel D after applying the thinning algorithm. (F) The final map of valley networks after applying the reconnection algorithm to the image shown in panel E.

tered out some pixels that are not part of the drainage, however, a significant number of spurious pixels still remains.

3.3 Masking and thinning

To eliminate the remaining spurious pixels we construct a mask designed to cover the craters, which are Martian landforms containing many non-valley features characterized by positive values of κ_t . The mask consists of two parts, the “deep flood” part, and the texture part. The deep flood mask is designed to eliminate interiors of the craters where the scalloped walls produce a series of alternating positive and negative curvature features (see Fig. 2B). Craters are enclosed topographic basins which when subject to unlimited rainfall would collect water and becomes lakes. This property suggests masking them by using the flooding algorithm mentioned in section 1, hence the name - deep

flood mask. The trick is to flag pixels in craters, but not the pixels in lesser depressions, that may constitute parts of drainage. To this end the two flood modifications of an original terrain are calculated. The full flood raises the elevation to the top off point, resulting in a completely drainable terrain with all pits filled. The shallow flood only fills pits with depths smaller than a given limit h , resulting in a terrain where smaller depressions are eliminated but large depressions are unchanged. We use $h = 100$ m in our calculations. The deep flood mask consists of pixels that are modified by the full flood but not modified by the shallow flood. This mask is shown in gray on Fig. 3C.

The walls of many craters are breached preventing them from being flooded to their rims. The exposed walls are masked by texture mask. Terrain texture is surrogated by standard deviation of elevations, SD , calculated over a circular moving windows of radius equal to 20 pixels. The texture mask consists of pixels that are characterized by $SD > SD_{th}$. We use $SD_{th} = 130$ m in our calculations. The texture mask is shown in black on Fig. 3C. Comparison of Fig. 3C with Fig. 2 shows that the total mask is very effective in flagging non-degraded craters. Fig. 3D shows the result of applying the mask to the binary image shown in Fig. 3B. Removal of circular segments and masking craters succeeds in separating the valleys from other landforms fulfilling the curvature criterion. The remaining image is subjected to thinning operation (Band, 1986) for skeletonization - reducing all lines to a single pixel thickness. Fig. 3E shows the thinned segments of an image representing the drainage network.

3.4 Reconnection

The thinned pixels are connected using a method similar to that described by Tarboton and Ames (2001). The method uses elements of the drainage directions algorithm. We calculate drainage directions for the terrain modified by the shallow flood. Using the shallow flood insures the flow continuity but prevents large craters from becoming the part of drainage. The pixels designated as parts of drainage (black on Fig. 3E) are given the weight 1 and all remaining pixels are given the weight 0. Using those weights the contributing area is calculated for every pixel in the site. Here, the contributing area of a pixel, $F(x, y)$, is a total number of weights collected from pixels that can be linked to it through an uninterrupted chain of slope directions. Thus, only pixels morphologically designated as “drainage” contribute. The drainage network is delineated as those pixels in the raster of the contributing areas that fulfill the criterion $F(x, y) > F_{th}$. We use $F_{th} = 5$ pixels in our calculations. This procedure yields connected and organized network. One problem that we have encounter with this method is that it sometimes produces long spurious channels in order to connect isolated convex pixels located on plateaus. To

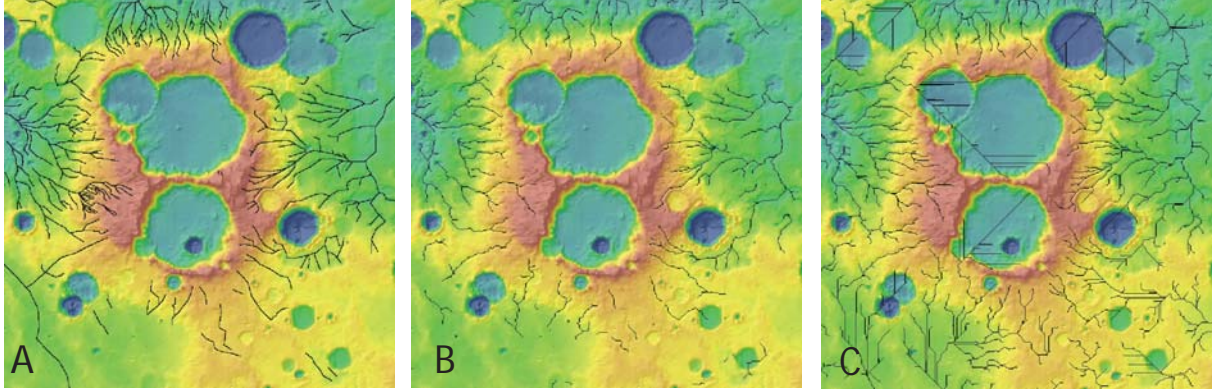


Fig. 4. (A) Manually mapped valley networks in the Pollack test site superimposed on a shaded relief of topography colored using elevation values. Blue-to-red gradient corresponds to low-to-high elevations. (B) The map of valley networks generated by our algorithm. (C) Valley networks mapped using drainage direction algorithm with $F_{\text{th}} = 200$ pixels.

prevent such occurrences we have introduced a concept of decay. Contributions to F from neighboring pixels are decreased by the decay factor d . This way a channel is allowed to “fade away” when there is no longer enough convex pixels to sustain it. We use $d = 0.95$ in our calculations. Fig. 3F shows the drainage network that results from our reconnection procedure. This constitutes the final output of our algorithm.

4 Comparison to manual maps

Fig. 4 shows visual comparison of the network delineated by our algorithm (panel B) to the manually mapped network (A), and the network delineated by drainage directions algorithm (C). The drainage directions algorithm uses constant contributing area criterion with an arbitrarily selected value of $F_{\text{th}} = 200$ pixels that results in a network that most resembles the mapped network. Network delineated by our algorithm closely matches the mapped network. Of particular interest is the ability of our algorithm to reproduce spatial variability of network density, or to delineate valleys only in those places where they are seen on images. In contrast, network delineated by the drainage directions algorithm contains many spurious valleys. Mapped network appears denser than delineated network, especially up the slopes of large craters. We attribute this difference to fivefold difference in resolution between images, used for manual mapping, and DEMs, used by our algorithm. The network delineated by the drainage directions algorithm also appears to be denser than our network, however, recall that its density depends on an arbitrarily set value of F_{th} (Tarboton and Ames, 2001; Stepinski and Collier, 2004).

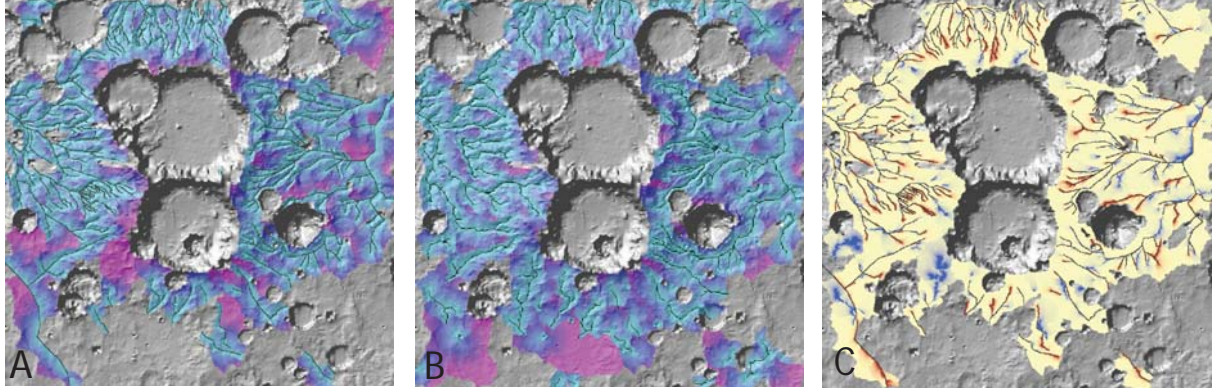


Fig. 5. (A) Watershed of manually mapped valley networks in the Pollack test site superimposed on a shaded relief of topography. The blue-to-pink gradient corresponds to low-to-high values of l . (B) Watershed of valley networks delineated by our algorithm. (C) Common watershed, red-yellow-blue gradient corresponds to negative-zero-positive values of drainage closeness parameter ξ .

There is no standard method to assess the quality of delineated network. Networks are difficult objects to compare quantitatively. For example, we consider manually mapped valleys to constitute the “ground truth,” however, they have been drawn by hand on top of images and may not conform exactly to topographic valleys in a coregistered DEM. The measure of quality of delineated network should not be sensitive to the offset between the two networks caused by such mapping imperfections. Our measures of delineation quality are based on the concept of pixel-to-valley length, l . The length $l(x, y)$ is defined by following the steepest descent path downslope until a channeled pixel is reached (see, for example, Tucker et al. (2001)). All pixels that have a finite value of l constitute a watershed of the network. The remaining pixels are either inside closed depressions (craters) or drain to a channel located outside the site. One quantitative measure of delineation quality is the amount of overlap between the watersheds of delineated and mapped networks. We introduce two measures of such overlap. FN (“false negative”) is the number of pixels that are in the mapped watershed but not in the delineated watershed. FP (“false positives”) is the number of pixels that are in the delineated watershed but not in the mapped watershed. Both, FN and FP , are normalized by the area of mapped watershed and expressed in terms of percentages. Small values of FN and FP correspond to high degree of watersheds overlap. Fig. 5A shows a watershed (164067 pixels) of manually mapped network in the test site, whereas Fig. 5B shows a watershed (202601 pixels) of network delineated by our algorithm. The overlap factors are $FN = 2.4\%$ and $FP = 25\%$. A similar analysis for network delineated by the drainage direction algorithm yields $FN = 0.4\%$ and $FP = 89\%$.

At a pixel level, the quality of network delineation may be measured by comparing the value of its pixel-to-valley length, l_{alg} , to an analogous length, l_{map} ,

Table 2
Quality factors for delineated networks

site #	Name	$L_{\text{alg}}/L_{\text{map}}$	FN	FP	$\langle \xi \rangle$	$p(\xi \leq 1)$	$p(\xi \leq 2)$
1	Locras Valles	0.59	0.4	28.0	0.05	52.0	66.0
2	Pollack	0.52	2.4	25.0	-0.57	57.0	71.0
3	Evros Vallis West	0.76	2.3	47.0	0.66	52.0	67.0
4	Evros Vallis North	0.82	2.2	60.0	1.7	45.0	61.0
5	Dawes East	0.56	1.6	29.0	0.59	48.0	64.0
6	Millochou West	0.52	1.0	24.0	0.51	58.0	71.0
7	Millochou South	0.58	1.8	36.0	-0.003	59.0	71.0
8	Naktong Vallis	1.17	3.6	51.0	3.57	52.0	66.0

calculated using the mapped network. We introduce a drainage closeness parameter $\xi(x, y) = (l_{\text{map}} - l_{\text{alg}})/\text{Min}[l_{\text{map}}, l_{\text{alg}}]$. Small values of $|\xi|$ indicate high degree of correspondence between the two networks and good quality of delineation algorithm. Figs. 5A and B shows spatial distributions of l_{map} and l_{alg} in our test site. The range of l_{map} is 0 - 77 km, and the range of l_{alg} is 0 - 101 km. Fig. 5C shows spatial distribution of ξ calculated on the common watershed (160133 pixels) of mapped and delineated networks. Most pixels are depicted in yellow indicating small values of $|\xi|$ and thus high correspondence between delineated and mapped networks. Red pixels are located in places where mapped network is denser, and blue pixels are located in places where delineated network is denser. Additional delineation quality factors can be derived from statistics of ξ . We calculate $\langle \xi \rangle$, $p(|\xi| \leq 1)$ and $p(|\xi| \leq 2)$. The last two variables are percentages of pixels in the common watershed that have values of ξ within indicated range. They measure the correspondence between the two networks over the entire watershed, large values indicate high correspondence. For the network delineated for our test site $\langle \xi \rangle = -0.57$, $p(|\xi| \leq 1) = 57\%$ and $p(|\xi| \leq 2) = 71\%$. For comparison, network delineated using the drainage directions algorithm yields $\langle \xi \rangle = 1.73$, $p(|\xi| \leq 1) = 51\%$ and $p(|\xi| \leq 2) = 67\%$. Thus, on the common watershed, the correspondence of both delineated networks to the mapped network are similar, it is in the watershed overlapping factors that our algorithm has a decisive edge.

In addition to the Pollack test site, we have applied our delineation algorithm to the seven other test sites listed in Table 1. The quality factors for all test sites are shown in Table 2. The third column gives the ratio of the total length of valleys delineated by the algorithm, L_{alg} to the total length of mapped valleys, L_{map} . In most cases $L_{\text{alg}}/L_{\text{map}} < 1$ indicating that the algorithm delineated less valleys than was mapped. The exception is the Naktong Vallis site, that also happen to be the largest of the eight sites. Large sites

are particularly challenging for manual mapping because the tedious character of such work may result in some valleys being left out. The fourth and fifth columns give values of FN and FP , respectively. These values imply that, despite their smaller total lengths, the delineated networks have larger watersheds than mapped networks. This is because delineated networks benefit from topographic information and are more connected and organized than mapped networks. The sixth column gives the average value of drainage closeness parameter ξ . For example, the value $|\xi| = 1$ implies that, on average, the difference in length between the drainage paths to the two networks is equal to the length of the smaller path. The small values of $\langle \xi \rangle$ indicate that the two networks are, overall, close to each other on the common watershed. The last two columns give the values of $p(|\xi| \leq 1)$ and $p(|\xi| \leq 2)$ that measure the concentration of ξ around an ideal value of $\xi = 0$. The difference between the lengths of two drainage paths is smaller than the length of the smaller path for $\sim 50\%$ of pixels located in the common watershed. The difference between the lengths of two drainage paths is smaller than twice the length of the smaller path for $\sim 60 - 70\%$ of pixels located in the common watershed.

5 Discussion

Automatic delineation of valley networks on Mars presents a unique challenge. Despite visual resemblance to terrestrial river systems, valley networks lack spatial integration and are less organized. This renders the standard methods for drainage delineation unusable for valley networks applications. The problem is especially acute when we are interested in mapping entire regions of Mars displaying high spatial variability of drainage density. The algorithm presented in this paper has been especially designed for mapping the valley networks. Recognizing relative lack of connectivity of Martian surface, we have based our algorithm on terrain morphology instead of terrain connectivity. In addition, we have found necessary to employ a series of image processing steps to separate valleys from other landforms having the same morphological signature. The code and its documentation is available from the authors upon request.

Visual comparison between networks delineated and mapped for eight test sites testifies to the high quality of our algorithm. In the paper such comparison is shown only for one site (Fig. 4), but the correspondence between the two networks in this site is typical for all other sites. This is further substantiated by quality factors listed in Table 2, with factors having similar values for all eight sites. Although our analysis is based on the assumption that manually mapped networks constitute the ground truth, the comparison calculations reveals limitations of manual, image-based mapping. First, manual mapping is done without the benefit of topographical information yielding networks

that do not conform to topography. As a result, a watershed calculated using a mapped network is incomplete. Based on the values of FP in Table 2, about a third of the watershed is “lost,” mostly due to lack of conformity with topography. On the other hand, the delineated network ensures such conformity. Thus, for any watershed analysis usage of delineated network is preferable even where mapped network is available. Second, a quality of manual mapping may depend on the site’s size. For most of the test sites, which are relatively small, our algorithm finds less valleys than was mapped (see the values of $L_{\text{alg}}/L_{\text{map}}$ in Table 2) because mapping was done using higher resolution data. However, for the largest site (Naktong Vallis) the algorithm delineated more valleys than was mapped. As manual mapping is a tedious work, larger sites may be mapped less completely than smaller sites. Of course, the quality of automatic delineation is independent of a site’s size. Thus, for mapping large regions, automatic delineation is not only more practical, but also may result in more complete map. Our method should find an immediate application for studies of processes that control origin and evolution of Martian drainage basins. Density and character of valley networks changes from one region of Mars to another. Our algorithm can provide detailed maps of valley networks in these regions to be used in looking for correlation between drainage density and other landscape characteristics.

Of course, the algorithm is also applicable to terrestrial terrain. We have used the USGS global digital topography data (GTOP30) with 30-arc second (~ 1 km) resolution to construct two DEMs, one covering an area of $\sim 5.4 \times 10^6$ km² in North America, and another covering an area of $\sim 9.2 \times 10^6$ km² in the north part of Africa. We have applied our algorithm to these two DEMs “as is”, without changing the values of parameters tuned for Martian applications. The resulting drainages are similar to those available from USGS’ HYDRO1k database, however, we have noticed that in some parts of the Sahara Desert our algorithm produced no streams (none are seen on images) whereas the HYDRO1k database (produced using the drainage directions algorithm) shows the presence of streams. Detailed analysis of our algorithm performance on terrestrial landscapes is beyond the scope of the present paper. The image processing part of our algorithm was operational for terrestrial calculations, but yielded, as expected, minimal modifications. Without the image processing part, our algorithm is quite similar to that described by Tarboton and Ames (2001), although the method of flagging convex pixels is different. Additional analysis is necessary to determine whether our algorithm, as applied to terrestrial terrain, provides any advantages over the Tarboton and Ames (2001) algorithm.

Acknowledgements

This research was supported by NSF under grant IIS-0430208 and by NASA under grant NNG05GM31G. This research was conducted at the Lunar and Planetary Institute, which is operated by the USRA under contract CAN-NCC5-679 with NASA. This is LPI Contribution No. 1308.

References

- Baker, V.R., Partridge, J.B., 1986, Small Martian Valleys: Prestine and Degraded Morphology, *J. Geophys. Res.*, 91, B3, 3561-3572.
- Band, L.E., 1986, Topographic partition of watersheds with digital elevation models, *Water Resources Research*, 22(1), 15-24.
- Cabrol, N.A., Grin, E.A., 2001, Composition of the drainage network on Early Mars, *Geomorphology*, 37, 269-287.
- Carr, M.C., 1995, The Martian drainage system and the origin of valley networks and fretted channels, *J. Geophys. Res.*, 100, E4, 7479-7507.
- Carr, M.C., 1996, *Water on Mars*, Oxford University Press, New York.
- Chang, F., Chen, C.J., Lu, C.J., 2004, A Linear Time Component Labeling Algorithm Using Contour Tracing Technique, *Computer Vision and Image Understanding*, 93(2), 206-220.
- Howard, A.D., 1992, A detachment-limited model of drainage basin evolution, *Water Resources Research*, 30, 2261-2285.
- Hynek, B.M., Phillips, R.J., 2001, Evidence for Extensive denudation of the Martian Highlands, *Geology*, vol. 29, no. 5, 407-410.
- Masursky, H., 1973, An overview of geologic results from Mariner 9, *J. Geophys. Res.*, 78, 4009-4030.
- Michielsen, K., De Raedt, H., 2001, Integral-geometry morphological image analysis, *Physics Reports*, 347, 461-538.
- Milton, D.G., 1973, Water and processes of degradation in the martian landscape, *J. Geophys. Res.*, 78, 4037-4047.
- Mitasova, K., Hofierka, J., 1993, Interpolation by Regularized Spline with Tension: II. Application to Terrain Modeling and Surface Geometry Analysis, *Mathematical Geology*, 25, 657-669.
- Montgomery, D.R., Dietrich, W.E., 1992, Channel Initiation and the problem of landscape scale, *Science*, 255, 826-830.
- O'Callaghan, J.F., Mark, D.M., 1984, The extraction of drainage networks from digital elevation data, *Computer Vision, Graphics and Image Processing*, 28, 328-344.
- Peucker, T.K., Douglas, D.H., 1975, Detection of surface-specific points by local parallel processing of discrete terrain elevation data, *Comput. Graphics Image Process.*, 4, 375-387.

- Plaut, J.J., and the 2001 Mars Odyssey team, 2003, Mars Odyssey Science: The First Year and Beyond, In Lunar and Planetary Science XXXIV, #1919, Lunar and Planetary Institute, Houston (CD-ROM).
- Roering, J.J., Kirchner, J.W., Dietrich, W.E., 1999, Evidence for nonlinear, diffusive sediment transport on hillslopes and implications for landscape morphology, *Water Resources Research*, 35(3), 853-870.
- Smith, D., Neumann, G., Arvidson, R.E., Guinness, E.A., Slavney, S., 2003, Mars Global Surveyor laser altimeter mission experiment gridded data record, NASA Planetary Data System, MGS-M-MOLA-5-MEGDR-L3-V1.0.
- Stepinski, T.F., Collier, M.L., 2004, Extraction of Martian valley networks from digital topography. *Journal of Geophysical Research* 109, E11005.
- Tarboton, D.G., Bras, R.L., Rodriguez-Iturbe, I., 1991, On the extraction of channel networks from digital elevation data, *Hydrologic processes*, 5(1), 81-100.
- Tarboton, D.G., Bras, R.L., Rodriguez-Iturbe, I., 1992, A physical basis for drainage density, *Geomorphology*, 5, 59-76.
- Tarboton, D.G., Ames, D.P., 2001, Advances in the mapping of flow networks from digital elevation data, in *World Water and Environmental Resources Congress*, Orlando, Florida, May 20-24.
- Tucker, G.E., Catani, F., Rinaldo, A., Bras, R.L., 2001, Statistical analysis of drainage density from digital terrain data, *Geomorphology* 36, 187-202, 2001.
- van Gasselt, S., Hauber, E., Reiss, D., Hoyer, M., Matz, K.D., Jaumann, R., 2002, A channel database based on a morphometric classification of valley networks, In *Lunar and Planetary Science XXXIII*, Abstract # 1949.